Hemolytic Lectin CEL-III Heptamerizes via a Large Structural Transition from α-Helices to a β-Barrel during the Transmembrane Pore-Formation Process

Hideaki Unno, Shuichiro Goda, and Tomomitsu Hatakeyama[1]

From the Laboratory of Biomolecular Chemistry, Graduate School of Engineering, Nagasaki University, 1-14 Bunkyo-machi, Nagasaki 852-8521, Japan

Running title: Crystal structure of the pore-forming CEL-III heptamer

To whom correspondence should be addressed: Tomomitsu Hatakeyama, Laboratory of Biomolecular Chemistry, Graduate School of Engineering, Nagasaki University, 1-14 Bunkyo-machi, Nagasaki 852-8521, Japan, Tel.: +81-95-819-2686; Fax: +81-95-819-2686; Email: thata@nagasaki-u.ac.jp

Keywords: carbohydrate; lectin; membrane; toxins; X-ray crystallography; β-barrel; hemolysin; oligomer; pore-forming toxin

Background: The hemolytic lectin CEL-III self-oligomerize upon binding to cell surface carbohydrates to form transmembrane pores.
Results: The CEL-III oligomer's crystal structure revealed a membrane-inserted pore structure.
Conclusion: CEL-III forms a heptamer containing a long β-barrel as the pore structure, resulting from a large conformational changes.
Significance: The heptameric structure of CEL-III provides insights into the action mechanisms of pore-forming proteins.

ABSTRACT

CEL-III is a hemolytic lectin isolated from the sea cucumber *Cucumaria echinata*. This lectin is composed of two carbohydrate-binding domains (domains 1-2) and one oligomerization domain (domain 3). After binding to the cell surface carbohydrate chains through domains 1-2, domain 3 self-associates to form transmembrane pores, leading to cell lysis or death, which resembles other pore-forming toxins of diverse organisms. To elucidate the pore-formation mechanism of CEL-III, the crystal structure of the CEL-III oligomer was determined. The CEL-III oligomer has a heptameric structure with a long β-barrel as a transmembrane pore. This β-barrel is composed of 14 β-strands resulting from a large structural transition of α-helices accommodated in the interface between domains 1-2 and domain 3 in the monomeric structure, suggesting that the dissociation of these α-helices triggered their structural transition into a β-barrel. After heptamerization, domains 1-2 form a flat ring, in which all carbohydrate-binding sites remain bound to cell surface carbohydrate chains, stabilizing the transmembrane β-barrel in a position perpendicular to the plane of the lipid bilayer.

Many bacteria produce pore-forming toxins (PFTs)[2], which are secreted as soluble proteins that bind to target cell surface receptors and oligomerize to form transmembrane pores in the lipid bilayer. Such a pore-formation in the cell membrane disrupts various cellular functions or causes cell death. Among PFTs, α-hemolysin and γ-hemolysin from *S. aureus* (1,2) have been extensively studied in terms of the structural changes that occur during pore-formation in target cell membranes. Their pore-formation processes proceed through binding to the cell membrane and self-association to form heptamers or octamers, followed by

conformational changes to form a transmembrane β-barrel. Although both monomeric and oligomeric structures are available for γ-hemolysin, which enables a detailed examination of structural changes during pore-formation, there is a paucity of information for other PFTs that are postulated to undergo large conformational changes on the cell membrane, leading to the formation of the membrane-inserted oligomers.

PFTs also exist in eukaryotes. The most well-known examples are complement proteins (C6-C9) and perforin in the immune systems of higher vertebrates. These PFTs contain membrane attack complex/perforin (MACPF) domains, which form membrane-pores to lyse target cells or deliver other factors such as granzymes (3) into target cells to promote apoptosis. A mushroom lectin LSL is another example of a eukaryotic pore-forming toxin isolated as a hemolytic lectin (carbohydrate-binding protein) from the parasitic mushroom *Laetiporus sulphureus* (4). LSL is known to bind to Gal-containing carbohydrate chains as its receptors on cell surface. Interestingly, this protein shares structural similarities with the bacterial PFTs, aerolysin from *Aeromonas hydrophila* and ε-toxin from *Clostridium perfringens*.

CEL-III is a eukaryotic PFT that has been purified as a Ca^{2+}-dependent hemolytic lectin from the marine invertebrate *Cucumaria echinata* (sea cucumber) (5-7). While this lectin exhibits binding affinity for carbohydrates containing GalNAc and Gal at nonreducing ends, it also shows hemolytic and cytotoxic activities by forming pores in target cell membrane, which may contribute to defense against this animal's predators. CEL-III is composed of two ricin B-chain-like carbohydrate-recognition domains (domains 1-2) and a C-terminal domain (domain 3) that is responsible for oligomerization in target cell membranes. CEL-III binds to specific carbohydrate-chains on the target cell surface via five carbohydrate-binding sites in domains 1-2. This binding to the cell surface is assumed to promote conformational changes of domain 3 to expose its hydrophobic region including two α-helices (H8 and H9), which then leads to self-oligomerization and concomitant insertion into the cell membrane to form transmembrane pores (7,8). As shown for other PFTs, detailed analyses of the oligomerization mechanisms, including large conformation changes, are very important in elucidating the actions of PFTs. However, information that describes structural transitions during the oligomerization process is limited. This absence of structural data is due to the difficulties associated with the crystallization of the oligomeric forms of PFTs. We have previously found that CEL-III can oligomerize upon binding disaccharides containing β-galactoside structures, such as lactose (Galβ1-4Glc) and lactulose (Galβ1-4Fru) in aqueous solution under high salt concentration and high pH conditions. The size of this soluble oligomer was estimated to be a hexamer or heptamer on SDS-PAGE, suggesting its structural similarity with the pore-forming oligomers in the erythrocyte membrane (7). We have recently crystallized this soluble oligomers in the presence of the detergent *n*-dodecyl-β-D-maltoside (DDM), and found the presence of a 7-fold rotational symmetry in its oligomeric structure (9). In the present study, we have determined the crystal structure of this CEL-III oligomer, which reveals the heptameric transmembrane pore structure. In comparison with the monomeric structure, an extensive secondary structural change of α-helices to β-strands is suggested to play an important role in the pore-formation process in target cell membrane.

EXPERIMENTAL PROCEDURES

Purification of CEL-III – Specimens of *Cucumaria echinata* were collected from the Sea of Genkai, Fukuoka, Japan. CEL-III was purified from the body fluid of *C. echinata* by chromatography using lactose-Cellulofine, GalNAc-Cellulofine and Sephadex G-75 columns, essentially as described previously (5,10).

Preparation of the CEL-III oligomer—CEL-III oligomers were prepared

as described previously (7) with the following modifications: purified CEL-III monomer (2 mg/ml) was incubated in the presence of 1 M NaCl, 100 mM glycine-NaOH buffer (pH 10), 10 mM $CaCl_2$ and 100 mM lactulose at 25 °C for 2 h. After oligomerization, the protein was dialyzed against 10 mM Tris-HCl (pH 7.6), 150 mM NaCl and then solubilized with 0.1% DDM in the same buffer. The solubilized CEL-III oligomers were concentrated to 12 mg/ml using a 100-kDa cutoff membrane (Vivaspin, GE Healthcare Biosciences, Uppsala, Sweden). For stabilization, the CEL-III oligomers were incubated in 10 mM Tris-HCl (pH 7.6), 150 mM NaCl, 10 mM $CaCl_2$, 100 mM lactulose and 0.5% DDM at 20 °C for 1 h.

Small-Angle X-ray Scattering—SAXS measurements were done on the beamline BL-10C at the Photon Factory (Tsukuba, Japan). A wavelength of 1.488 Å and a specimen-to-detector distance of 958.8 mm were used, and all measurements were carried out at 25°C in a temperature-controlled cell holder. The time for SAXS analysis of CEL-III monomer and oligomer in the presence and absence of DDM solutions (concentration of about 3 mg/ml) were 120, 300 and 1200 s for each measurement. The radius of gyration (*Rg*), forward scattering intensity normalized with respect to the protein concentration (*J*(0)/*C*), molecular mass, and maximum particle dimension (D_{max}) (Table 1) were calculated as described in the previous paper (11).

Crystallization, crystal stabilization and derivatization—For crystallization, sitting drops of 4–8 μl sample were mixed with 2 μl of a solution containing 100 mM sodium acetate (pH 4.2), 100 mM $CdCl_2$ and 30% PEG400, and equilibrated by vapor diffusion against the same solution. Crystals grew within 2 weeks. For stabilization and cryo-protection of the crystals, the mother liquor was replaced by a cryo-stabilization solution of 100 mM sodium acetate (pH 4.2), 0.1 M $CdCl_2$, 10 mM $CaCl_2$, 100 mM lactulose and 35–45% PEG400. For heavy atom derivatization, crystals were soaked in a buffer containing 100 mM sodium acetate (pH 4.2), 0.1 M $CdCl_2$, 10 mM $CaCl_2$, 100 mM lactulose, 35% PEG400, 0.5% DDM and 2 mM K_2PtCl_4 for 12 h at 20 °C.

Data collection, structure determination and refinement—Native1 data were collected at beamline i03 of the Diamond light source (Harwell, UK), and native2 and Pt-derivative data were collected on BL-5A at the Photon Factory (Tsukuba, Japan). Data indexing, integration and scaling of native1 were carried out with the program HKL2000 (12), and that of native2 and the Pt-derivative were carried out with the CCP4 (13) programs Mosflm (14) and SCALA (15). Data collection statistics are summarized in the Table 2. All data sets belonged to space group *C*2 with one heptamer per asymmetric unit. native2 and the Pt-derivative data sets were used for phase calculation by single isomorphous replacement with anomalous scattering (SIRAS) using the program PHENIX (16). Phase improvement by density modification including non-crystallography symmetry (NCS) averaging was performed by the program PHENIX. The structure was built using the program COOT (17) and refined using Refmac (18), with 5% of the data set aside as a free set. During subsequent refinement, the native2 data set was replaced by the native1 data set. Lactulose models were fitted into the carbohydrate-binding sites based on the difference electron density map. NCS restraints were applied among 7 subunits throughout the refinement. The C_α atoms of domains 1-2 in monomeric and heptameric CEL-III were superimposed with the program LSQKAB (19). Superposition of the scaffold region in domain 3 of the CEL-III monomer into those in the heptamer was performed with the CCP4 program SUPERPOSE (20). The final model, comprising residues 1–432, agree with the crystallographic data with R_{free} and R_{work} of 27.3% and 24.0%, respectively (Table 2). All figures and movie were produced using the software PyMOL (http://www.pymol.org).

RESULTS AND DISCUSSION

Preparation and Crystallization of CEL-III Oligomers—CEL-III forms oligomers in aqueous solution upon binding of β-galactoside containing carbohydrates, such as lactose and lactulose, under high pH and high salt concentration conditions (7). These oligomers show a similar size on SDS-PAGE to those formed in the erythrocyte membrane during the hemolytic process. This suggests that CEL-III undergoes similar structural changes even in solution, triggered by the binding of specific carbohydrates, which may mimic the initial step of the action of CEL-III on target cell membranes. Although the soluble oligomers showed a band of 270 kDa, which corresponds to a hexamer on SDS-PAGE, their actual size in solution was estimated to be about 1 MDa. This size corresponds to a 21 mer by small-angle X-ray scattering measurements (21), suggesting that hexamers or heptamers further associate to form trimers through relatively weak interactions. These weak interactions were disrupted by detergents, such as Triton X-100 and SDS (11). For crystallization of CEL-III oligomers, DDM was found to yield good crystals, which diffracted to 2.9 Å resolution (9). The sizes of the CEL-III monomer and oligomers determined by small-angle X-ray scattering are presented in Table 1. While CEL-III monomer and the oligomer in the absence of DDM gave molecular masses of 4.7×10^4 Da and 9.8×10^5 Da, respectively, which are comparable to previous data (11, 21), the addition of 0.5% DDM resulted in a decrease in size to 3.4×10^5 Da. These results suggest that the dissociation of large oligomers to core oligomers occurs through the disruption of hydrophobic interactions between core oligomers. The crystals of CEL-III oligomers were prepared in the presence of 0.5% DDM by the sitting drop vapor diffusion method, and they were used for the X-ray diffraction data collection.

Overall structure of CEL-III heptamer—The crystal structure of the CEL-III oligomer was solved at 2.9 Å resolution using SIRS method for phase calculation with Pt-derivative crystals.. As shown in Fig. 1, CEL-III oligomer forms a drawing-pin-like heptamer with a height and diameter of 115 and 175 Å, respectively. There is a long 14-stranded β-barrel structure running along the 7-fold symmetry of the heptamer, which may form a pore when inserted in the target cell membrane. Although domains 1-2 of the heptamer maintain the basic monomeric CEL-III structures (PDB codes 1VCL, 2Z48, and 2Z49) (6,22) (Fig. 2), domain 3 undergoes drastic structural changes upon heptamerization, leading to the formation of bundle and stem regions that construct a central axis (Fig. 3*A*). The stem region adopts a long 2-stranded β-sheet, which further assemble to form the 14-stranded β-barrel of the heptamer. The bundle region interacts with each other at the top of the β-barrel, stabilizing its pore structure. The β-barrel has a height and diameter of 75 and 25 Å, respectively, which are sufficient dimensions to make a transmembrane pore that allows passage of small ions and molecules across the cell membrane. The length of the β-barrel of the CEL-III heptamer is relatively long when compared with those of other β-PFTs (e.g., ~50 Å in α-hemolysin from *S. aureus*). On the outer surface of the β-barrel, several hydrophobic residues, especially valine residues, alternately appearing in the sequence (23) are exposed, whereas hydrophilic side chains mostly face towards the inside the β-barrel. In addition, three aromatic residues, Phe314, Trp353, and Phe336, exist at the upper (Phe314 and Trp353) and bottom (Phe336) regions of the outer surface of the β-barrel. Such a distribution of aromatic residues in membrane-penetrating β-barrels (aromatic belt) was suggested to be involved in the interaction with the lipid head groups (24,25). In addition to the interactions between domain 3 from each protomer, carbohydrate-binding domains 1-2 also stabilize the pore structure by forming a large outer ring on the cell surface (Fig. 1*A*). In the crystal structure, their carbohydrate-binding sites are occupied by lactulose molecules added for the oligomerization process (Fig. 4). All the carbohydrate-binding sites are located on the undersurface of the outer ring, facing

the postulated cell membrane, as shown in Fig. 1*A*. This suggests that the transmembrane pore in the lipid bilayer may be stabilized by the outer ring composed of domains 1-2 binding to cell surface carbohydrate chains. An electrostatic potential analysis shows that the lower surface of the outer ring has a strong negative potential (Fig. 5). This is partly because of acidic residues coordinating 35 Ca^{2+} ions, which are essential for the recognition of galactose residues. The inner surface of the pore shows a characteristic distribution of electrostatic potentials, in which, the lower two-thirds and upper one-third have strong positive and negative potentials, respectively.

Structural transition during heptamerization—The structural transition of the CEL-III monomer to its heptamer during the hemolytic process requires extensive conformational changes in domain 3. Domain 3 of monomeric CEL-III contacts the side of domains 1-2 with its two α-helices (H8 and H9) accommodated in the cleft between them (Fig. 3*B*). Upon heptamerization, it dissociates from domains 1-2, transforming to the bundle and stem regions that self-associate to form a central membrane-spanning axis (Fig. 3*A*). During such a heptamerization process, the two α-helices transform to two long β-strands that further assemble into the 14-stranded β-barrel. This is a remarkable difference from conformational transitions observed for other β-PFTs, as represented by α-hemolysin and γ-hemolysin from *S. aureus* (1,2), which form β-barrels in the membrane through the assembly of the pre-stem regions made of a β-hairpin that has originally formed a 3-stranded β-sheet on the side of a soluble monomer. As we reported previously (8), domain 3 is found to oligomerize spontaneously once it is cleaved from domains 1-2. This finding suggests that oligomerization of CEL-III is triggered by the exposure of an internal face of domain 3 to the solvent, which may be promoted by the conformational changes induced by binding of domains 1-2 to the carbohydrate chains as CEL-III receptors on the cell surface. It seems possible that such conformational changes are induced by lateral movements of glycoproteins or glycolipids, to which domains 1-2 are bound. In addition, internal structural changes in domains 1-2 (Fig. 4*B* and *C*) may also be involved in the dissociation of domain 3, supported by the finding that binding of a specific carbohydrate such as lactulose and lactose under high pH and high salt conditions promoted heptamerization of CEL-III (7).

As shown in Fig. 6, conformational changes of domain 3 during heptamerization occur in the structural units, which are referred to as terminal (residues 284–291 and 420–432), scaffold (residues 292–308, 362–386 and 401–419), wrapping (residues 387–400) and stem (residues 309–361) regions (Fig. 6*B*). While residues 284–291 in the terminal region are situated 16 Å apart from residues 420–432 in monomeric CEL-III (Fig. 6*A*), after dissociation of domain 3 from domains 1-2, residues 284–291 connected to domain 2 are trailed along the movement of domain 3 and approach residues 420–432. By contrast, the stem region, originally composed of two α-helices, three short β-sheets and loop structures in monomeric CEL-III, converts to a long 2-stranded β-sheet (β-hairpin), which contributes to the 14-stranded β-barrel as a transmembrane pore formed by the heptamer. This transition includes a drastic secondary structural switch from α-helices to β-sheets, and a concomitant increase in main chain hydrogen bonds from 30 to 54, among which 28 are between adjacent protomers (Fig. 7*A* and *B*). The wrapping region (residues 387–400) comprising two β-strands and a connecting loop also changes largely its conformation and hydrogen bond pairing (Fig. 7*C* and *D*).

Although the terminal, wrapping and stem regions accounting for 72% of the total residues in domain 3 undergo extensive structural changes, the remaining (scaffold) region basically retains its original conformation during the heptamerization process. The surface of the scaffold region is mostly buried inside the CEL-III monomer, becoming exposed to make significant interactions with adjacent protomers after

heptamerization. It seems likely that the scaffold region plays a central role in constructing a heptameric ring in an early stage of the heptamerization process. Formation of the heptameric ring through scaffold regions between adjacent protomers is followed by the conformational changes in the wrapping and stem regions to form the β-barrel structure that inserts into the lipid bilayer. The importance of the scaffold region in pore-formation has been suggested by the finding that the site-directed mutagenesis of Arg378 to alanine resulted in an almost complete loss of hemolytic activity of CEL-III (26). In the heptameric structure, Arg378 forms ionic and hydrogen bonds with Asp373 and Asn369, respectively, between the scaffold regions of adjacent protomers (Fig. 8*A*) to stabilize the ring structure. It seems very likely that the formation of the ring structure composed of the scaffold region precedes the formation of the β-barrel in the lipid bilayer. When domain 3 in monomeric CEL-III is fitted to those of the heptameric structure so that their corresponding scaffold regions are superimposed, no collision occurs among these domains (Fig. 8*B*). This fact also supports the assumption that a heptameric ring as a prepore (27,28) may be formed prior to β-barrel formation by the stem region after binding to the target cell surface. After prepore formation, the transmembrane pore composed of the β-barrel may be formed through a number of hydrogen bonds between adjacent β-strands, leading to a stable heptamer structure that is resistant to heat and detergent treatments (7).

Proposed mechanism of pore-formation—Based on these findings, we propose a spontaneous pore-formation mechanism of CEL-III (Fig. 9 and supplemental Movie S1) comprising 4 steps: 1) binding to the specific carbohydrate-chains on the cell membrane, 2) domain movements, 3) heptamerization and 4) β-barrel formation. In step 1), CEL-III monomers bind to Gal/GalNAc-containing carbohydrate chains, such as those of glycolipids, on the target cell membrane via the five carbohydrate-binding sites in domains 1-2 (Fig. 9*A*). In step 2), movement of the domains exposes the internal surface of domain 3. This structural change exposes the scaffold region that is buried in monomeric CEL-III (Fig. 9*B*), and induces self-association through their exposed hydrophobic surfaces (step 3, Fig. 9*C*). In step 4), the 14-stranded β-barrel is formed by association of 2-stranded β-sheets contributed from each protomer (Fig. 9*D*). During this β-barrel formation process, 26 hydrogen bonds in the two α-helices and three short β-sheets disappear in a protomer, while 50 hydrogen bonds are newly formed in the two long amphipathic β-sheets (Fig. 7*A* and *B*). This gives a net increase of 24 hydrogen bonds per protomer and such an increase may provide the driving force for the extensive structural changes of the stem region. The pore-structure of heptameric CEL-III shows conspicuous differences from those of the other β-PFTs, whose three-dimensional structures are known; the CEL-III heptamer contains a long β-barrel of 75 Å in length, whereas those of other β-PFTs are typically ~50 Å in length. Additionally, the CEL-III heptamer forms a large flat ring of a diameter of 175 Å comprising domains 1-2, which contains 35 carbohydrate-binding sites. Such a large ring contacting the surface of the cell membrane might be advantageous for stabilizing the long membrane-spanning β-barrel perpendicularly embedded into the lipid bilayer.

Comparison with other proteins—Although CEL-III shows similarities in the size of pores with α-hemolysin (1), γ-hemolysin (2) from *Staphylococcus aureus*, *Vibrio cholerae* cytolysin (29), aerolysin from *Aeromonas hydrophila* (30), and the anthrax toxin from *Bacillus anthrasis* (28), its secondary structural change from α-helices to β-strands to form a membrane-spanning β-barrel rather resembles those of the CDC (cholesterol-dependent cytolysin) family proteins and MACPF (membrane attack complex/perforin) domains (27,31), which form larger pores. These proteins are produced by various pathogenic gram-positive bacteria or cytotoxic T-cells

and natural killer cells in mammalian immune systems, respectively. These proteins also form pores composed of membrane-spanning β-barrels, which are derived from α-helices in soluble monomeric form. Besides these proteins, secondary structural changes from α-helices to β-strands are also known to be a critical step for the action of the proteins responsible for conformational diseases, such as Alzheimer's, Parkinson's and prion diseases (32), which are assumed to be mediated by the deposition of aggregates resulting from structural conversion from α-helices in soluble proteins to insoluble β-sheet aggregates. Further detailed analyses for the structural changes of CEL-III during heptameric pore-formation should provide important clues not only to the action mechanisms of PFTs, but also to the mechanism of aggregation of the proteins responsible for conformational diseases.

REFERENCES

1. Song, L., Hobaugh, M. R., Shustak, C., Cheley, S., Bayley, H., and Gouaux, J. E. (1996) Structure of staphylococcal α-hemolysin, a heptameric transmembrane pore. *Science* **274**, 1859-1866
2. Yamashita, K., Kawai, Y., Tanaka, Y., Hirano, N., Kaneko, J., Tomita, N., Ohta, M., Kamio, Y., Yao, M., and Tanaka, I. (2011) Crystal structure of the octameric pore of staphylococcal γ-hemolysin reveals the β-barrel pore formation mechanism by two components. *Proc. Natl. Acad. Sci. U.S.A.* **108**, 17314-17319
3. Voskoboinik, I., Smyth, M. J., and Trapani, J. A. (2006) Perforin-mediated target-cell death and immune homeostasis. *Nat. Rev. Immunol.* **6**, 940-952
4. Mancheño, J. M., Tateno, H., Goldstein, I. J., Martínez-Ripoll, M., and Hermoso, J. A. (2005) Structural analysis of the *Laetiporus sulphureus* hemolytic pore-forming lectin in complex with sugars. *J. Biol. Chem.* **280**, 17251-17259
5. Hatakeyama, T., Kohzaki, H., Nagatomo, H., and Yamasaki, N. (1994) Purification and characterization of four Ca^{2+}-dependent lectins from the marine invertebrate, *Cucumaria echinata*. *J. Biochem.* **116**, 209-214
6. Uchida, T., Yamasaki, T., Eto, S., Sugawara, H., Kurisu, G., Nakagawa, A., Kusunoki, M., and Hatakeyama, T. (2004) Crystal structure of the hemolytic lectin CEL-III isolated from the marine invertebrate *Cucumaria echinata*: implications of domain structure for its membrane pore-formation mechanism. *J. Biol. Chem.* **279**, 37133-37141
7. Hatakeyama, T., Furukawa, M., Nagatomo, H., Yamasaki, N., and Mori, T. (1996) Oligomerization of the hemolytic lectin CEL-III from the marine invertebrate *Cucumaria echinata* induced by the binding of carbohydrate ligands. *J. Biol. Chem.* **271**, 16915-16920
8. Kouzuma, Y., Suzuki, Y., Nakano, M., Matsuyama, K., Tojo, S., Kimura, M., Yamasaki, T., Aoyagi, H., and Hatakeyama, T. (2003) Characterization of functional domains of the hemolytic lectin CEL-III from the marine invertebrate *Cucumaria echinata*. *J. Biochem.* **134**, 395-402
9. Unno, H., Hisamatsu, K., Nagao, T., Tateya, Y., Matsumoto, N., Goda, S., and Hatakeyama, T. (2013) Crystallization and preliminary crystallographic study of oligomers of the haemolytic lectin CEL-III from the sea cucumber *Cucumaria echinata*. *Acta Crystallogr. F Struct. Biol. Cryst. Commun.* **69**, 416-420
10. Hatakeyama, T., Nagatomo, H., and Yamasaki, N. (1995) Interaction of the hemolytic lectin CEL-III from the marine invertebrate *Cucumaria echinata* with the erythrocyte membrane. *J. Biol. Chem.* **270**, 3560-3564
11. Goda, S., Sadakata, H., Unno, H., and Hatakeyama, T. (2013) Effects of detergents on the oligomeric structures of hemolytic lectin CEL-III as determined by small-angle X-ray scattering. *Biosci. Biotechnol. Biochem.* **77**, 679-681
12. Otwinowski, Z., and Minor, W. (1997) Processing of X-ray diffraction data collected in oscillation mode. *Methods Enzymol.* **276**, 307-326
13. Collaborative Computational Project, N. (1994) The CCP4 suite: programs for protein crystallography. *Acta Crystallogr. D Biol. Crystallogr.* **50**, 760-763
14. Leslie, A. G. (2006) The integration of macromolecular diffraction data. *Acta Crystallogr. D Biol. Crystallogr.* **62**, 48-57
15. Evans, P. (2006) Scaling and assessment of data quality. *Acta Crystallogr. D Biol. Crystallogr.* **62**, 72-82
16. Adams, P. D., Afonine, P. V., Bunkóczi, G., Chen, V. B., Davis, I. W., Echols, N., Headd, J. J., Hung, L. W., Kapral, G. J., Grosse-Kunstleve, R. W., McCoy, A. J., Moriarty, N. W., Oeffner, R., Read, R. J., Richardson, D. C., Richardson, J. S., Terwilliger, T. C., and

Zwart, P. H. (2010) PHENIX: a comprehensive Python-based system for macromolecular structure solution. *Acta Crystallogr. D Biol. Crystallogr.* **66**, 213-221
17. Emsley, P., Lohkamp, B., Scott, W. G., and Cowtan, K. (2010) Features and development of Coot. *Acta Crystallogr. D Biol. Crystallogr.* **66**, 486-501
18. Murshudov, G. N., Vagin, A. A., and Dodson, E. J. (1997) Refinement of macromolecular structures by the maximum-likelihood method. *Acta Crystallogr. D Biol. Crystallogr.* **53**, 240-255
19. Kabsch, W. (1976) A solution for the best rotation to relate two sets of vectors. *Acta Crystallogr.* A **32**, 922–923
20. Krissinel, E., and Henrick, K. (2004) Secondary-structure matching (SSM), a new tool for fast protein structure alignment in three dimensions. *Acta Crystallogr. D Biol. Crystallogr.* **60**, 2256-2268
21. Fujisawa, T., Kuwahara, H., Hiromasa, Y, Niidome, T, Aoyagi, H., and Hatakeyama, T. (1997) Small-angle X-ray scattering study on CEL-III, a hemolytic lectin from Holothuroidea *Cucumaria echinata*, and its oligomer induced by the binding of specific carbohydrate. *FEBS Lett.* **414,** 79-83
22. Hatakeyama, T., Unno, H., Kouzuma, Y., Uchida, T., Eto, S., Hidemura, H., Kato, N., Yonekura, M., and Kusunoki, M. (2007) C-type lectin-like carbohydrate recognition of the hemolytic lectin CEL-III containing ricin-type β-trefoil folds. *J. Biol. Chem.* **282**, 37826-37835
23. Hisamatsu, K., Unno, H., Goda, S., and Hatakeyama, T. (2009) Roles of the valine clusters in domain 3 of the hemolytic lectin CEL-III in its oligomerization and hemolytic abilities. *Protein Pept. Lett.* **16**, 411-414
24. Killian, J. A., and von Heijne, G. (2000) How proteins adapt to a membrane-water interface. *Trends Biochem. Sci.* **25**, 429-434
25. Montoya, M., and Gouaux, E. (2003) β-barrel membrane protein folding and structure viewed through the lens of α-hemolysin. *Biochim. Biophys. Acta* **1609**, 19-27
26. Hisamatsu, K., Nagao, T., Unno, H., Goda, S., and Hatakeyama, T. (2013) Identification of the amino acid residues involved in the hemolytic activity of the *Cucumaria echinata* lectin CEL-III. *Biochim. Biophys. Acta* **1830**, 4211-4217
27. Tilley, S. J., Orlova, E. V., Gilbert, R. J., Andrew, P. W., and Saibil, H. R. (2005) Structural basis of pore formation by the bacterial toxin pneumolysin. *Cell* **121**, 247-256
28. Lacy, D. B., Wigelsworth, D. J., Melnyk, R. A., Harrison, S. C., and Collier, R. J. (2004) Structure of heptameric protective antigen bound to an anthrax toxin receptor: a role for receptor in pH-dependent pore formation. *Proc. Natl. Acad. Sci. U.S.A.* **101**, 13147-13151
29. De, S., and Olson, R. (2011) Crystal structure of the *Vibrio cholerae* cytolysin heptamer reveals common features among disparate pore-forming toxins. *Proc. Natl. Acad. Sci. U.S.A.* **108**, 7385-7390
30. Parker, M. W., Buckley, J. T., Postma, J. P., Tucker, A. D., Leonard, K., Pattus, F., and Tsernoglou, D. (1994) Structure of the *Aeromonas* toxin proaerolysin in its water-soluble and membrane-channel states. *Nature* **367**, 292-295
31. Rosado, C. J., Buckle, A. M., Law, R. H., Butcher, R. E., Kan, W. T., Bird, C. H., Ung, K., Browne, K. A., Baran, K., Bashtannyk-Puhalovich, T. A., Faux, N. G., Wong, W., Porter, C. J., Pike, R. N., Ellisdon, A. M., Pearce, M. C., Bottomley, S. P., Emsley, J., Smith, A. I., Rossjohn, J., Hartland, E. L., Voskoboinik, I., Trapani, J. A., Bird, P. I., Dunstone, M. A., and Whisstock, J. C. (2007) A common fold mediates vertebrate defense and bacterial attack. *Science* **317**, 1548-1551
32. Toyama, B. H., and Weissman, J. S. (2011) Amyloid structure: conformational diversity and consequences. *Annu. Rev. Biochem.* **80**, 557-585

Acknowledgments– We thank the staff of i03 at the Diamond Light Source and BL-5A at the Photon Factory for developing an excellent beamline and support with data collection. This study was performed under the approval of the Photon Factory Adivisory Committee (Proposal Numbers 2011G535 and 2013G027)

FOOTNOTES

*This work was supported by a Grant-in-Aid for Scientific Research (C) to TH (50228467) and Grants-in-Aid for Young Scientists (B) to HU (10452872) and SG (00346587) from the Japan Society for the Promotion of Science (JSPS).
The atomic coordinates and structure factors for CEL-III heptamer has been deposited in the Protein Data Bank, www.pdb.org (PDB code 3W9T).
[1]To whom correspondence may be addressed: Laboratory of Biomolecular Chemistry, Graduate School of Engineering, Nagasaki University, 1-14 Bunkyo-machi, Nagasaki 852-8521, Japan, Tel.: +81-95-819-2686; Fax: +81-95-819-2686; Email: thata@nagasaki-u.ac.jp
[2]The abbreviations used are: PFT, pore-forming toxin; DDM, *n*-dodecyl-β-D-maltoside; SIRAS, single isomorphous replacement with anomalous scattering; SAXS, Small-angle X-ray scattering

FIGURE LEGENDS

FIGURE 1. **Crystal structure of CEL-III heptamer.** Side (*A*) and bottom (*B*) views of the CEL-III heptamer in ribbon representation. Each subunit is shown in a different color. Lactulose molecules bound to CEL-III are shown in orange sticks. Ca^{2+} and Mg^{2+} ions are indicated in green and light blue spheres, respectively.

FIGURE 2. **Comparison of the structures of domains 1 and 2.** *A*, superposition of domain 1 in the monomer (blue) and the protomer (red). *B*, superposition of domain 2 in the monomer (blue) and the protomer (red). Lactulose molecules bound to the protomer are shown as stick models. Ca^{2+} and Mg^{2+} ions are shown as spheres. Residues with a C_α deviation above 1.5 Å are indicated by arrows.

FIGURE 3. **Comparison of the structures of the protomer of the heptameric CEL-III with the monomeric CEL-III.** Bottom (Left) and side (Right) views of a protomer of the heptameric CEL-III (*A*) are compared with the monomeric CEL-III/methyl-α-D-galactopyranoside complex (*B*) (PDB code 2Z49) (22) in the same orientation with respect to their domain 2. Domains 1-2 are shown in blue and yellow, respectively. Bundle and stem regions derived from domain 3 are shown in green and red, respectively. Ca^{2+} and Mg^{2+} ions are shown as purple and green spheres, respectively. Lactulose in (*A*) and methyl-α-D-galactopyranoside in (*B*) are shown as orange sticks.

FIGURE 4. **Lactulose bound to heptameric CEL-III.** *A*, $F_o - F_c$ omit electron density map (blue) for lactulose bound to subdomain 1α of the domain 1. The lactulose was omitted in the calculation of the $F_o - F_c$ omit map (blue). The omit map is contoured at 4σ. The Ca^{2+} ion mediating the binding of the lactulose is shown as a gray sphere. Binding of lactulose to subdomains 2α (*B*) and 2β (*C*) induced local structural changes, especially of Glu184 and Tyr222. A yellow dotted line between lactulose and Glu184 designates a hydrogen bond formed upon binding of lactulose.

FIGURE 5. **Surface representations of the CEL-III heptamer.** Electrostatic potential of the outer (*A*) and inner (*B*) surfaces was mapped from negative (red) to positive (blue). Strong negative potential in the undersurface facing the membrane surface indicated by arrows is partly due to acidic residues (Asp and Glu) coordinating Ca^{2+} ions. The inside of the pore shows strong negative and positive potentials in the upper and lower regions, respectively.

FIGURE 6. **Conformational change in domain 3 during the heptamerization process.** Domain 3 of monomeric CEL-III (*A*) is compared with that of heptameric CEL-III (*B*) in the same orientation. The corresponding regions (terminal, scaffold, wrapping, and stem regions) are indicated in different colors.

FIGURE 7. **Structural changes in the stem and wrapping regions for the pore formation.** The stem (*A*, *B*) and wrapping (*C*, *D*) regions in the monomer (*A*, *C*) and protomer (*B*, *D*) are shown in schematic representations. Intra- and inter-protomer hydrogen bonds forming the secondary structures are shown as yellow and orange dashed lines, respectively. The residues in the stem and wrapping regions are colored red and blue, respectively.

FIGURE 8. **Interactions between the protomers in heptamric CEL-III.** *A*, Arg378 in the right molecule and Asp373’ and Asn369’ in the left molecule (light blue) form ionic and hydrogen bonds (yellow dashed lines) to stabilize the interactions between the protomers. *B*, a postulated heptameric assembly model of domain 3, in which seven molecules of domain 3 of monomeric CEL-III are arranged in the positions corresponding to those of the CEL-III heptamer. Terminal, scaffold, wrapping, and stem regions are shown in yellow, gray, blue, and red, respectively.

FIGURE 9. **Proposed mechanism of pore-formation.** Binding of CEL-III monomer to Gal- or GalNAc-containing carbohydrate chains on the cell membrane induces movement of domain 3, thereby exposing the hydrophobic face of the scaffold region (*A*-*B*). This exposure of the hydrophobic face of the scaffold region leads to the formation of the heptameric ring as a pre-pore structure (*C*). The 14-stranded β-barrel elongates,penetrating the lipid bilayer, which is stabilized by the ring composed of domains 1-2 and the bundle region (*D*). Terminal, scaffold, wrapping, and stem regions are shown in yellow, gray, blue, and red, respectively.

TABLE 1. Structural parameters of monomeric and oligomeric CEL-III by SAXS

CEL-III	*Rg* (Å)	*J*(0)/*C*	Molecular mass (Da)	D_{max} (Å)
Monomer	24.2	45.9 (1)[a]	4.7×10^4	75
Oligomer	92.6	954 (20.8)	9.8×10^5	277
Oligomer + 0.5% DDM	61.7	332 (7.25)	3.4×10^5	177

[a]Values in the parenthesis indicate the ratio of *J*(0)/*C* to that of the monomer.

TABLE 2. Data collection and refinement statistics.

Crystal type	**native1**	**native2**	**Pt-derivative**
Data collection and processing statistics			
Space group	*C*2	*C*2	*C*2
Unit cell dimension (Å)			
a (Å)	219.8	218.3	217.5
b (Å)	228.7	230.7	231.6
c (Å)	133.0	133.6	133.7
β (°)	127.1	126.9	126.8
Wavelength (Å)	0.9763	1.000	1.000
Resolution (Å)	53.5–2.90 (3.06–2.90) [a]	50.0–3.30 (3.36–3.30)	50.0–4.50 (4.58–4.50)
Total reflections	441,835	557,027	213,116
Unique reflections	113,863	79,710	31,095
$I/\sigma I$	7.1 (2.0)	21.3 (5.1)	14.7(4.3)
Redundancy	3.9 (3.9)	7.0 (7.0)	6.9 (6.7)
Completeness (%)	98.6 (99.3)	98.7 (100)	99.5 (99.9)
R_{merge} [b] (%)	10.0 (41.1)	9.6 (48.5)	12.6 (47.4)
Number of HA sites			7
Refinement statistics			
Resolution	48.2–2.90		
Protein atoms	23191		
Ligand atoms	909		
Water molecule	75		
R_{work}/R_{free}(%)	24.0 / 27.3		
Root mean square deviations			
Bond lengths (Å)	0.009		
Bond angles (°)	1.551		
Ramachandran statistics			
residues in favoured region	96.0		
residues in allowed region	3.0		
residues in outlier region	1.1		

[a]The values in parentheses are for the highest resolution shell.
[b]$R_{merge} = 100\Sigma|I - \langle I\rangle|/\Sigma I$, where I is the observed intensity and $\langle I\rangle$ is the average intensity of multiple observations of symmetry-related reflections.

Figure 1

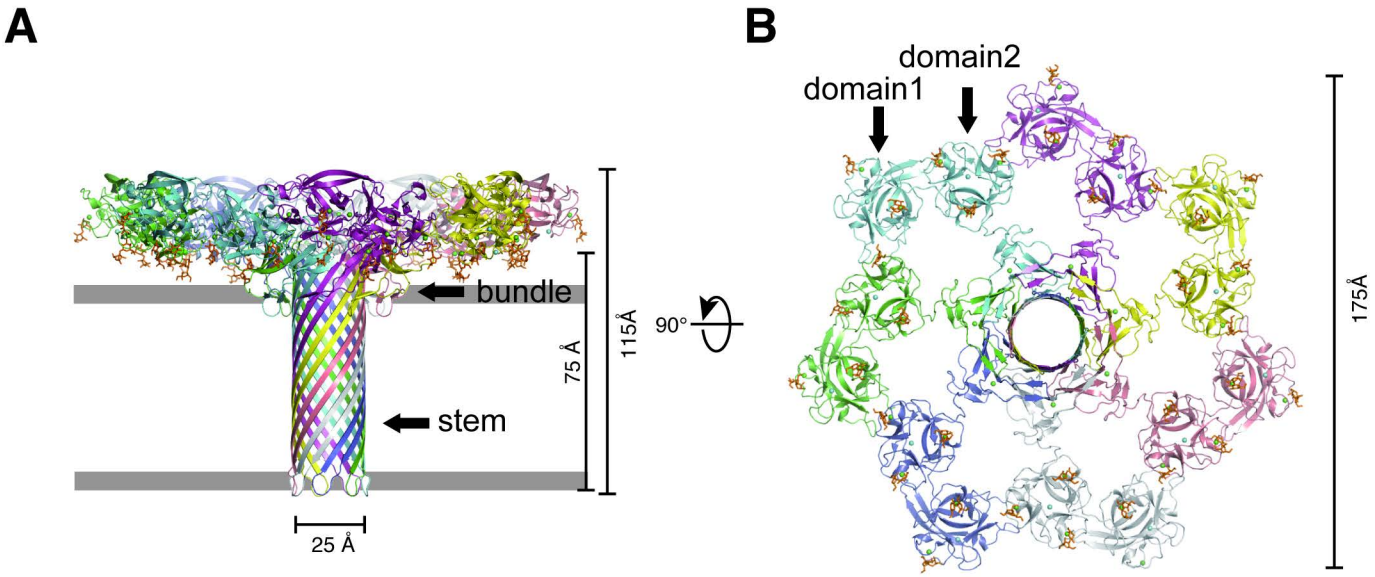

Figure 2

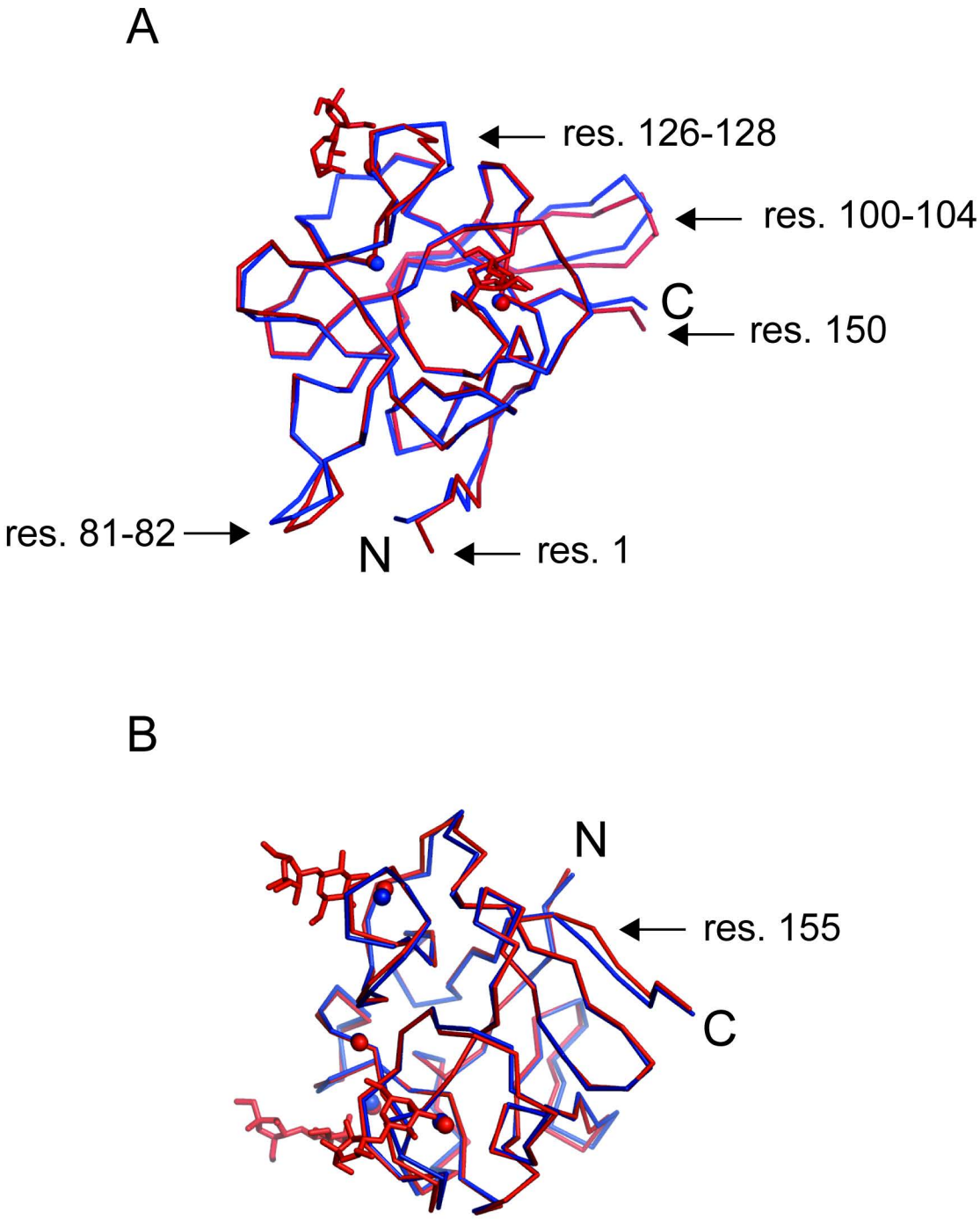

Figure 3

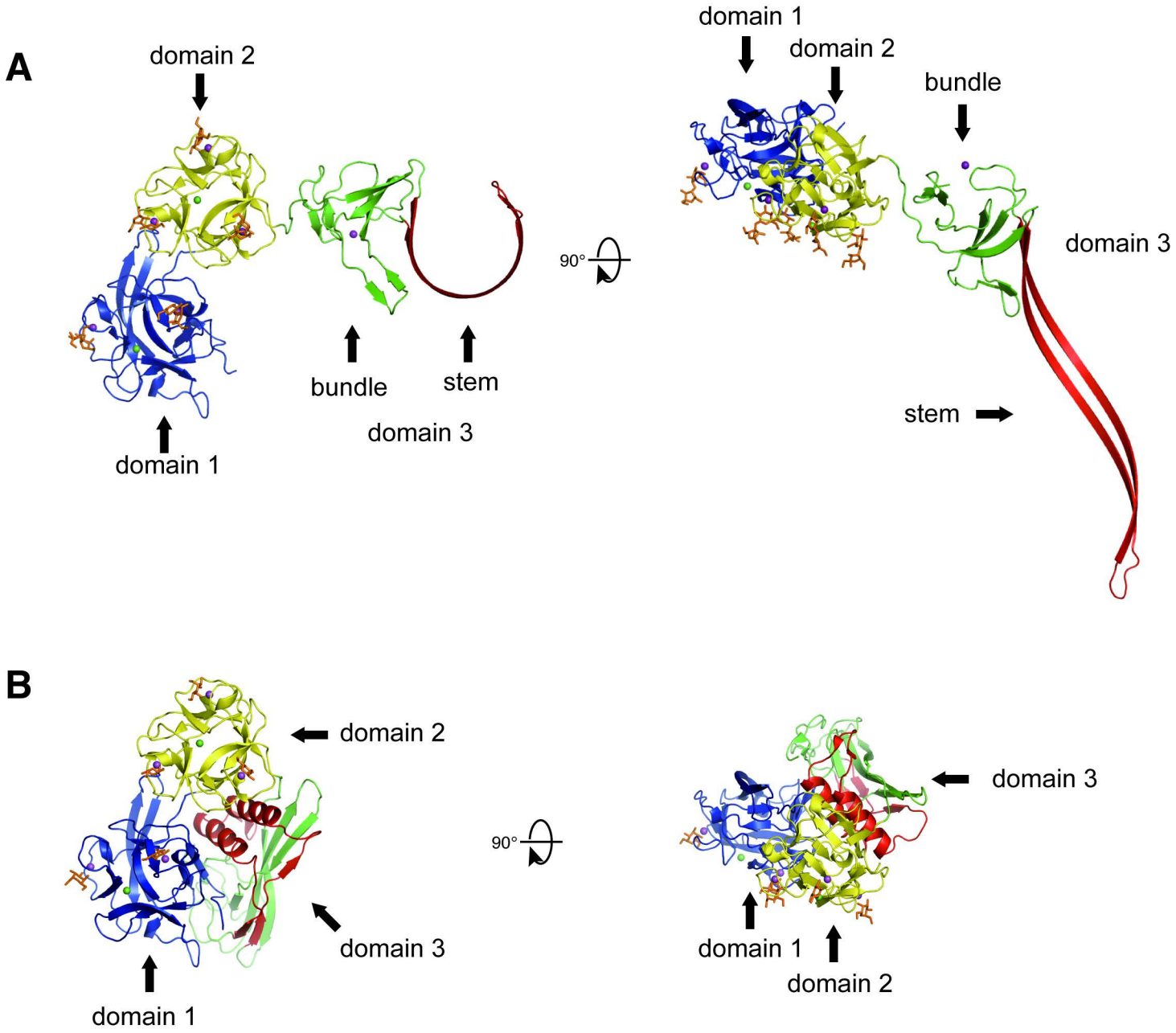
A
domain 2
domain 1
bundle
stem
domain 3
90°
domain 1
domain 2
bundle
domain 3
stem
B
domain 2
domain 3
domain 1
90°
domain 3
domain 1
domain 2

Figure 4

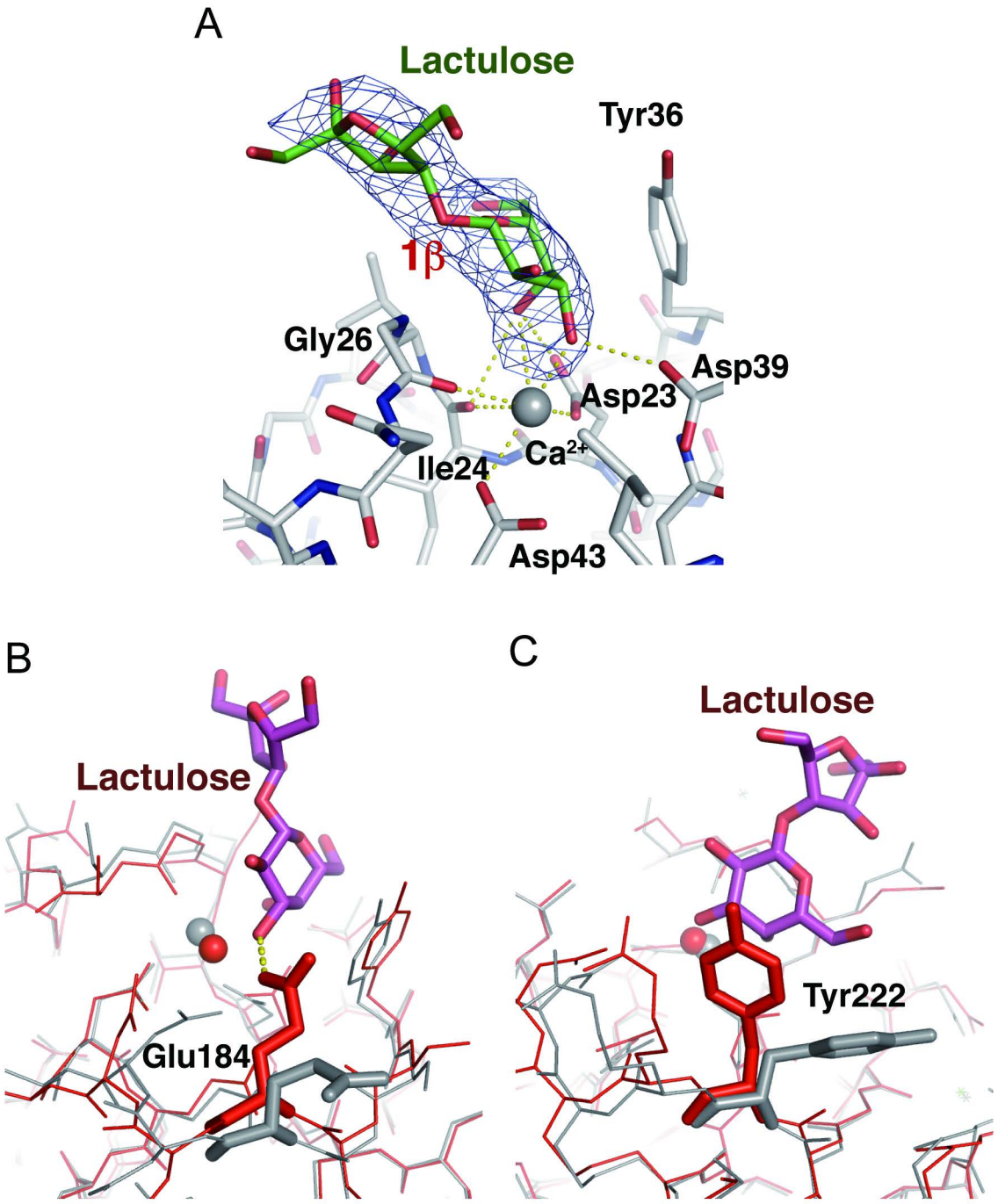
A
Lactulose
Tyr36
1β
Gly26
Asp39
Asp23
Ca2+
Ile24
Asp43
B
Lactulose
Glu184
C
Lactulose
Tyr222

Figure 5

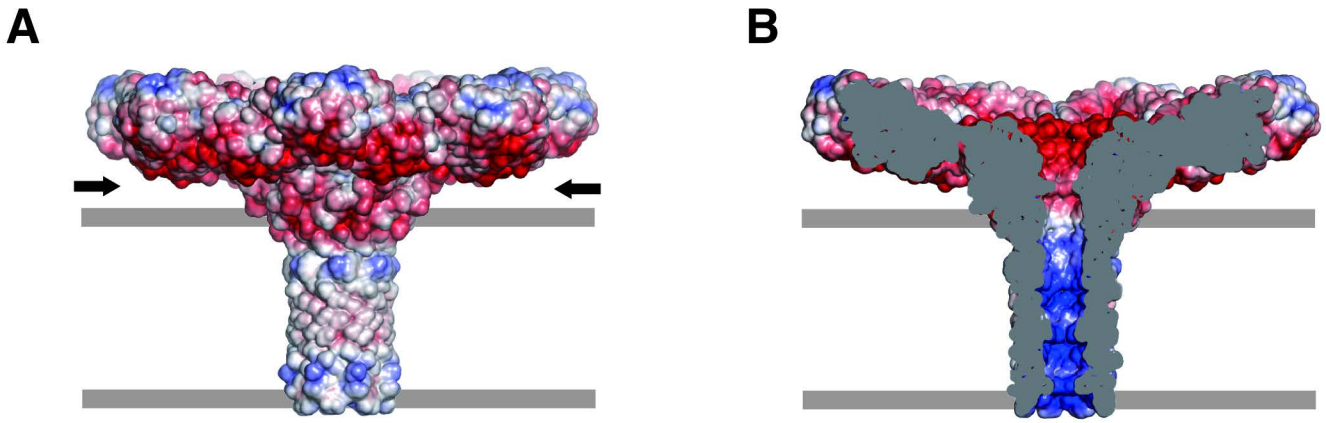

Figure 6

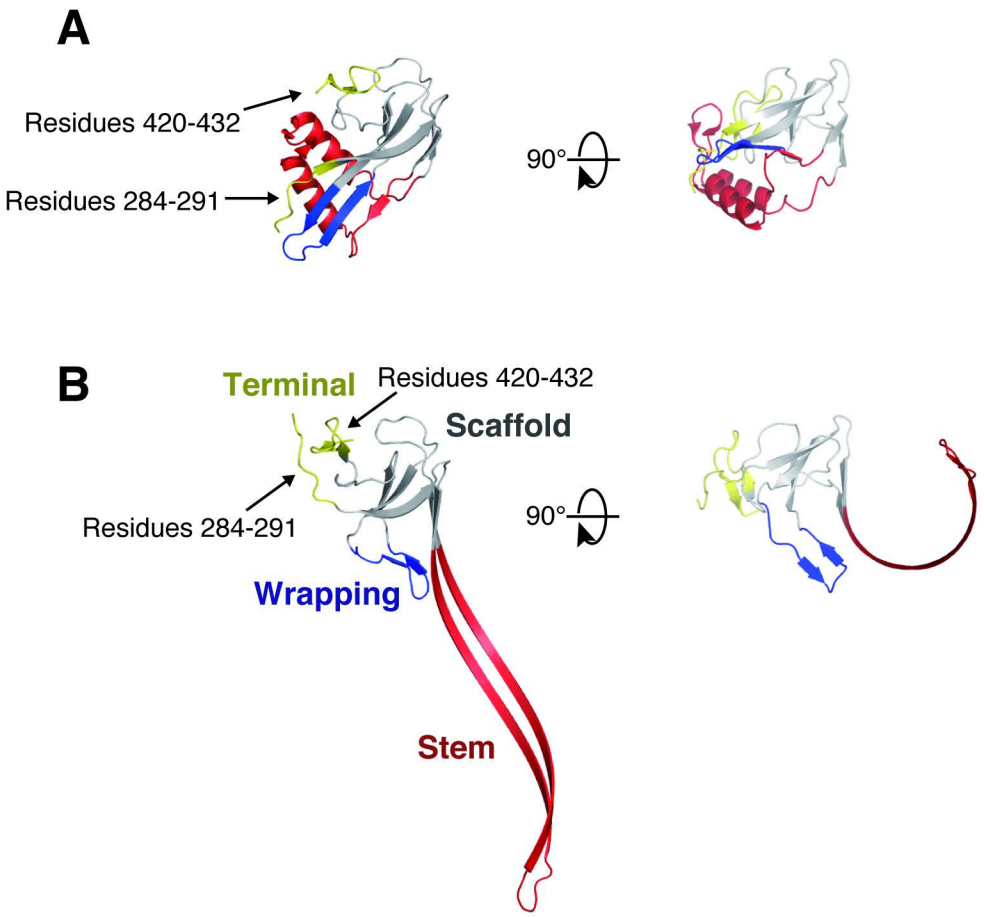
A
Residues 420-432
Residues 284-291
90°
B
Terminal
Residues 420-432
Scaffold
Residues 284-291
90°
Wrapping
Stem

Figure 7

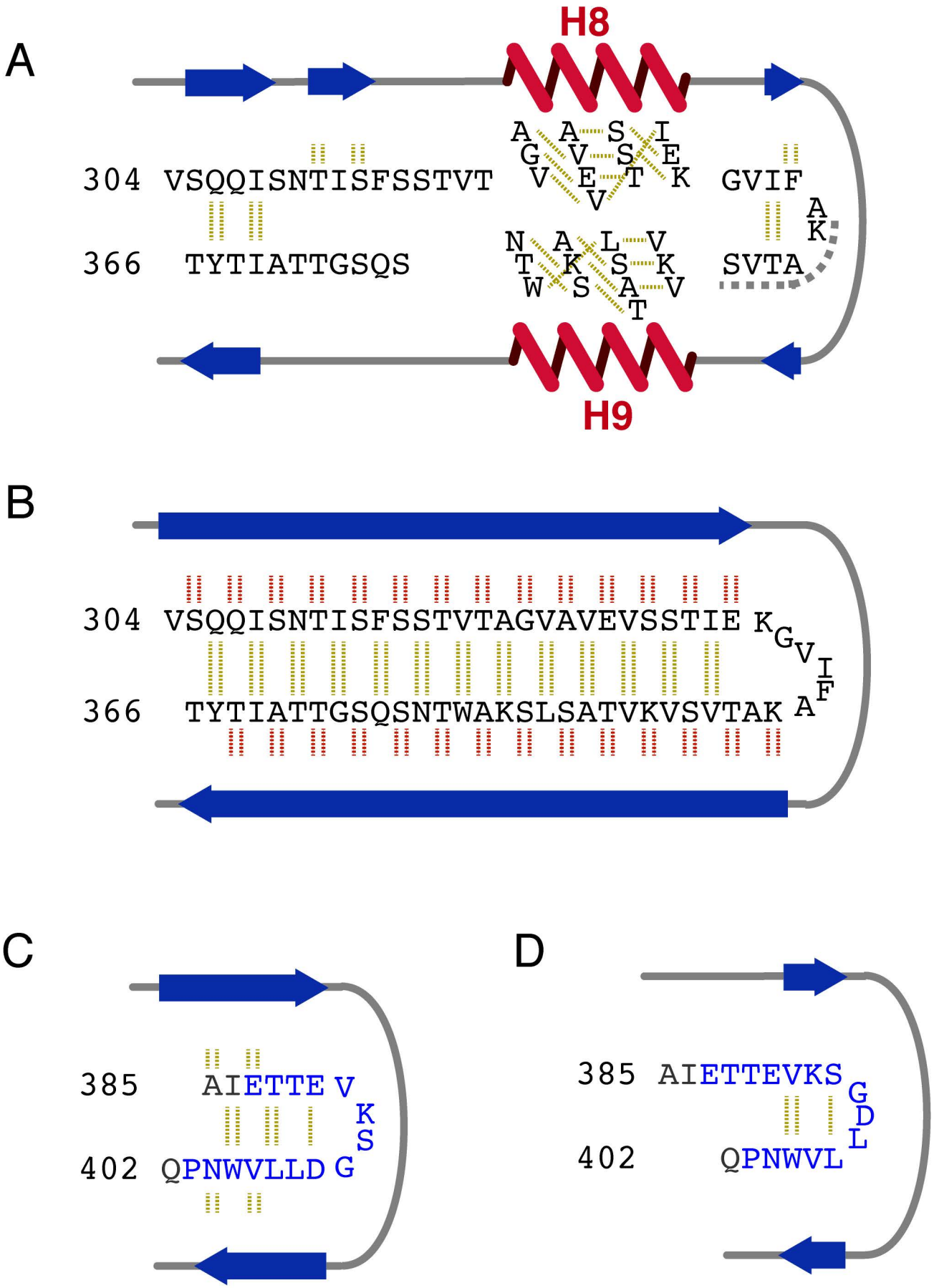
A
H8
H9
304 VSQQISNTISFSSTVT
366 TYTIATTGSQS
GVIF
SVTA
B
304 VSQQISNTISFSSTVTAGVAVEVSSTIE
366 TYTIATTGSQSNTWAKSLSATVKVSVTAK
C
385 AIETTE V
402 QPNWVLLD G
D
385 AIETTEVKS
402 QPNWVL

Figure 8

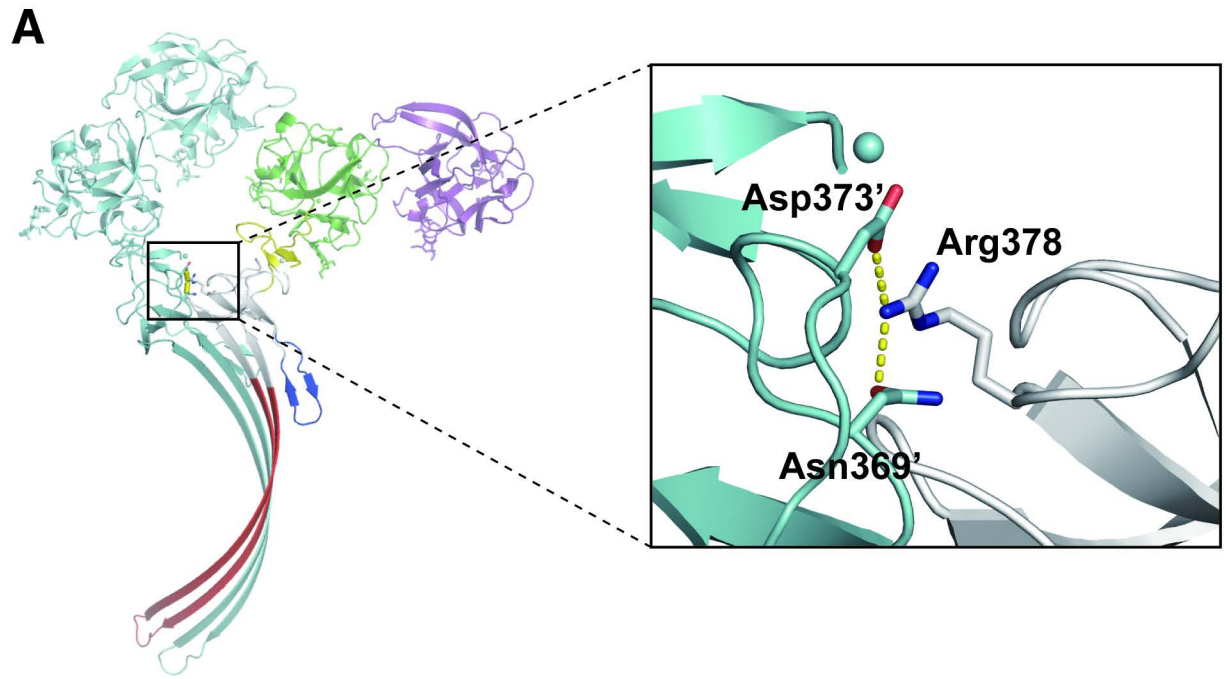

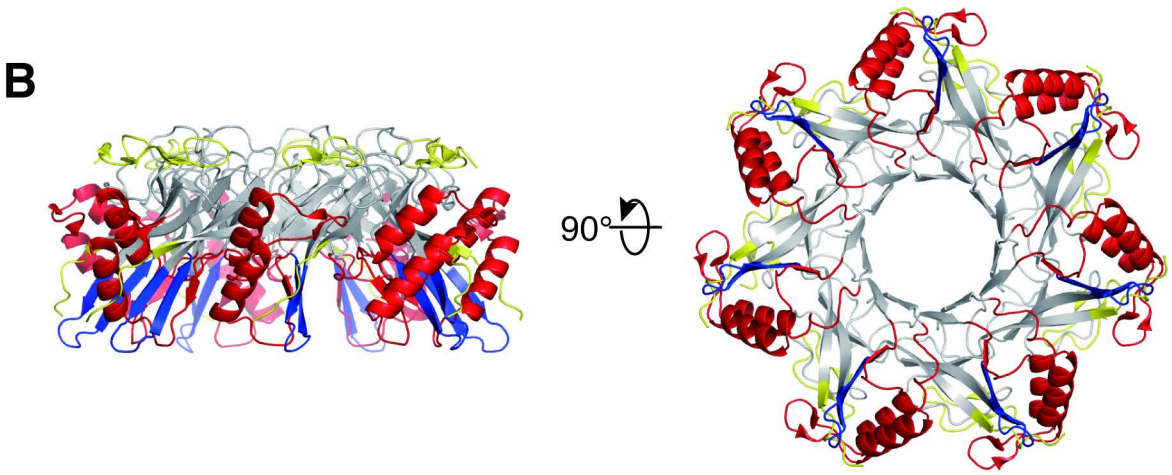

Figure 9